Catalysis Science & Technology

Elucidating the mechanism of the UiO-66-catalyzed sulfide oxidation: Activity and selectivity enhancements through changes in the node coordination environment and solvent

Journal:	*Catalysis Science & Technology*
Manuscript ID	CY-ART-06-2018-001139.R1
Article Type:	Paper
Date Submitted by the Author:	31-Aug-2018
Complete List of Authors:	Limvorapitux, Rungmai; Northwestern University, Dept. of Chemistry Chen, Haoyuan ; Rutgers, Mendonca, Matthew; Northwestern University Liu, Mengtan; Northwestern University, Dept. of Chemistry Snurr, Randall; Northwestern University, Department of Chemical & Biological Engineering Nguyen, SonBinh; Northwestern University, Dept. of Chemistry

Catalysis Science & Technology

ARTICLE

Elucidating the mechanism of the UiO-66-catalyzed sulfide oxidation: Activity and selectivity enhancements through changes in the node coordination environment and solvent

Received 00th January 20xx,
Accepted 00th January 20xx

DOI: 10.1039/x0xx00000x

www.rsc.org/

Rungmai Limvorapitux,[a] Haoyuan Chen,[b] Matthew L. Mendonca,[b] Mengtan Liu,[a] Randall Q. Snurr,[b,*] and SonBinh T. Nguyen[a,*]

Benzoic acid modulators that "cap" the Zr_6-oxo-hydroxo cluster nodes in UiO-66 metal-organic frameworks can be removed to increase the number of "open" sites (i.e., those that are terminated with [μ_1-OH + μ_1-OH_2]) up to 5 per node, enabling the "decapped" materials to exhibit enhanced catalytic activity in the oxidation of methyl phenyl sulfide. Computational modeling reveals that the labile Zr-μ_1-OH groups on these open sites are likely converted into Zr-μ_1-OOH species that are active in oxidizing the sulfide as well as its sulfoxide product. In solvents such as CH_3CN and CH_2Cl_2, the sulfoxide product can additionally replace the aquo ligands of the Zr-μ_1-OH_2 moieties to increase the concentration of the sulfoxide adjacent to the active Zr-μ_1-OOH species, resulting in overoxidation to the sulfone. However, the use of CH_3OH, a solvent that can compete with the sulfoxide and suppress this binding mode, can retard the overoxidation and lead to higher selectivities for the sulfoxide product.

Introduction

Zr_6-oxo-hydroxo clusters ($Zr_6(\mu_3\text{-}O)_4(\mu_3\text{-}OH)_4(OOCR)_x$), which can be stabilized by up to 12 carboxylate groups,[1-5] have long been used as building blocks for organic-inorganic hybrid materials[6, 7] and molecular magnets,[8, 9] as well as in catalysis.[10] When the carboxylate ligands are multitopic linkers, the Zr_6-oxo-hydroxo clusters can be connected together to form a broad range of metal-organic frameworks (MOFs),[11] such as the UiO,[12-14] PCN,[15-17] and NU[18, 19] families, among many others.[20-23] Within the UiO MOFs, UiO-66 (linker = 1,4-benzenedicarboxylate, BDC) was found to be catalytically active for the oxidation of sulfides[24-27] and for Lewis-acid-catalyzed reactions such as Friedel-Crafts benzoylation,[28] aldol condensation,[29] hydrolysis,[30, 31] transesterification,[32] and ring opening.[33, 34] While the catalytically active species in these reactions were assumed to be derived from the coordinatively unsaturated sites on the Zr_6-oxo-hydroxo nodes of the MOF,[25-27, 34-37] their nature remains ambiguous, particularly for sulfide oxidation where the unsaturated sites, as precatalysts, must be converted into the oxidation-active species.

In the oxidative desulfurization of fuels, where UiO-66 has been studied as a catalyst for the second processing stage[38] (H_2O_2-induced oxidation of the sulfide, Scheme 1), samples that are less-crystalline or have more defects[24, 26, 27] are often more active. While this has been attributed to the increased presence of coordinatively unsaturated node sites[25-27] and linker deficiencies,[24, 26, 27] previous studies employed widely different MOF preparations[24, 26, 27] that could manifest into large variations on the observed catalytic activities.[39-41] To this end, we were interested in the possibility of modulating the catalytic activity of UiO-66 in sulfide oxidation using only materials derived from a single preparation. We hypothesized that increasing the number of missing-linker[42] sites on the Zr_6-oxo-hydroxo nodes of UiO-66, as well as the accessibility of these sites, should lead to enhancements in catalytic activities. In combination with computational modeling and kinetic studies, this structure-function relationship study will allow us to establish the chemical identity of the active catalyst species in the UiO-66-catalyzed sulfide oxidation and propose a reasonable mechanism for the two steps of Scheme 1.

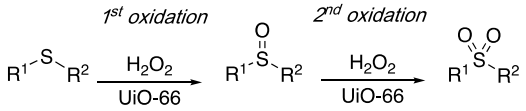

Scheme 1 The UiO-66-catalyzed oxidation of sulfide with H_2O_2 oxidant.

Missing-linker sites on the Zr_6-oxo-hydroxo nodes of UiO-66 MOFs are well-known to be capped with modulator-type carboxylate ligands during synthesis.[43] However, the capping is not perfect and the modulator can be lost or removed during modification (Scheme 2).[34, 37] Under these scenarios,

[a] Department of Chemistry and the Institute for Catalysis in Energy Processes, Northwestern University, 2145 Sheridan Road, Evanston, Illinois 60208. Email: stn@northwestern.edu.
[b] Department of Chemical and Biological Engineering, Northwestern University, 2145 Sheridan Road, Evanston, Illinois 60208. Email: snurr@northwestern.edu

†Electronic Supplementary Information (ESI) available. MOF characterization data (PXRD, N2 isotherms, NMR, SEM, and compositional data), catalysis and computational details, catalysis data, optimized structural data for key species, and additional discussion. See DOI: 10.1039/x0xx00000x

the missing-linker sites are assumed to be terminated with a combination of [Zr-μ_1-OH + Zr-μ_1-OH_2][44-46] (or [Zr-μ_1-Cl + Zr-μ_1-OH_2/neutral solvent][47, 48]). Such "open" sites are much more coordinatively labile than the *chelating* carboxylate-capped sites and can become active sites in catalysis.[43] Herein, we report the post-synthesis transformation of a single UiO-66 sample into a family of three UiO-66 materials with the number of open sites readily tuned from ~1 to 5 per node, while preserving the parent particle morphology. These materials were tested for sulfide oxidation in the presence of H_2O_2 (Scheme 1), where the MOF with more open sites indeed resulted in higher reaction rates for both sulfide and sulfoxide oxidation. Reactions in different solvents showed a high selectivity for the sulfoxide in CH_3OH, but in CH_3CN and CH_2Cl_2 the selectivity drops rapidly with increasing conversion.

Computational modeling provided support for a Zr-μ_1-OOH active species, generated from a μ_1-OH site that is capable of oxidizing sulfide to sulfoxide and further oxidation to the sulfone. Together, the experimental and computational results suggested a model where the sulfoxide product can bind to a Zr site adjacent to the active Zr-μ_1-OOH species in CH_3CN and CH_2Cl_2, leading to overoxidation. However, this effect is minimized in CH_3OH, which can interact strongly with the open sites on the nodes, reduce sulfoxide binding, and thus maintain good sulfoxide selectivity.

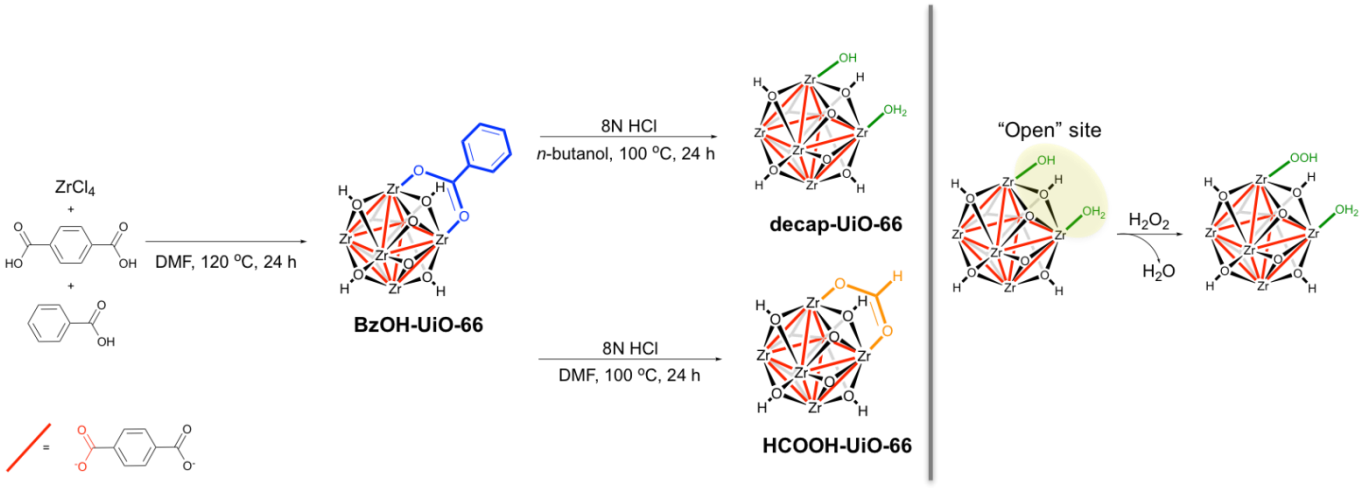

Scheme 2. The synthesis of the three isomorphic UiO-66 materials used in this work (left panel) and a proposal for the conversion of a Zr-μ_1-OH species in the open sites into active Zr-μ_1-OOH species (right panel). For simplicity, only one Zr_6-oxo-hydroxo node of each UiO-66 sample is shown here.

Results and discussion

Synthesis and characterization of the UiO-66 derivatives

As a prototypical MOF, crystalline UiO-66 nanoparticles have been synthesized under many different conditions, particularly with acid modulators[37, 49-51] that change the number of missing BDC linkers while maintaining well-defined crystal morphologies.[49, 51, 52] With benzoic acid (BzOH) modulators, the degree of missing-linker sites on the UiO-66 nodes can readily be tuned, up to ~4 missing-linker sites (or two BDC linkers) per node.[52] These missing-linker sites are presumably capped with the monocarboxylate anions of the acid modulators, which can then be decapped to yield [μ_1-OH + μ_1-OH_2][44-46] open sites. By using a large excess of benzoic acid modulator (BzOH/BDC = ~33)[49] (Scheme 2), we synthesized a parent **BzOH-UiO-66** material with ~3 BzOH-capped, 0.3 formic acid (HCOOH)-capped (see further discussion below), and ~1 open sites per node (Table 1, entry 2). To increase the number of open sites on the nodes, this **BzOH-UiO-66** was treated with HCl_{aq} in the presence of *n*-butanol to remove BzOH, resulting in **decap-UiO-66**, which had the same BDC linker/node composition as the parent material but with 4.6 times as many open sites (Table 1, entry 3).

Table 1. Composition of the three UiO-66 MOF derivatives and the Zr_6-oxo-hydroxo cluster used in this work.

Entry	MOF	Number per node[b]			Maximum number of open sites[d]
		BDC	BzOH	HCOOH	
1	"Ideal" **UiO-66**[a]	6	0	0	0
2	**BzOH-UiO-66**	3.9	2.9	0.3[c]	1.0
3	**decap-UiO-66**	3.7	0	0	4.6
4	**HCOOH-UiO-66**	3.7	0	3.9	0.7
5	Isolated Zr_6-oxo-hydroxo cluster	0	8.7	0	3.3

[a]The "ideal" UiO-66 structure is defined as a structure with the formula $Zr_6O_4(OH)_4(BDC)_6$, that has exactly 6 BDC linkers/node (i.e., no missing linker and no capping ligand; ESI,† Table S1). [b]Determined from ^{1}H NMR analyses of solutions of the digested MOFs. [c]Derived from the hydrolysis of DMF during the MOF synthesis. [d]Calculated by comparing to the "ideal" UiO-66 structure.

When the parent **BzOH-UiO-66** was subjected to the same HCl_{aq} treatment but in the presence of DMF, we obtained a **HCOOH-UiO-66** material with 3.9 HCOOH-capped and 0.7 open sites per node (Table 1, entry 4). Presumably, the HCOOH ligands came from the high-temperature acid-catalyzed hydrolysis of DMF[53] and readily bound to the nodes of UiO-66 to replace the BzOH capping ligands.[50, 51] The PXRD patterns

(ESI,† Fig. S6), BET areas (ESI,† Table S1), and SEM images (ESI,† Fig. S8) for **decap-UiO-66** and **HCOOH-UiO-66** are very similar to those of the parent **BzOH-UiO-66** MOF, confirming that the crystallinity, porosity, and morphology are preserved after both modifications. Together with the parent **BzOH-UiO-66**, these materials form a family of isomorphic MOFs with a relatively broad range of open sites (1-5) per node for us to explore in sulfide oxidation catalysis.

Selection of reaction system

As organic sulfides can be overoxidized to sulfone in the presence of excess H_2O_2, we used only a stoichiometric amount of H_2O_2 oxidant in our catalysis to limit this possibility.[54-56] We also chose methyl phenyl sulfide as a substrate that is known to give both sulfoxide and sulfone products[57, 58] during the oxidation, allowing us to delineate the activity and selectivity profiles of our catalysts. While dibenzothiophene and its derivatives have been previously used in UiO-66-catalyzed sulfide oxidation experiments,[24-27] sulfoxide products were not observed, presumably because they readily undergo oxidation to the sulfone.[59] Lastly, we employ CH_3OH, CH_3CN, and CH_2Cl_2 as solvents in our study to explore the differences between a solvent that is capable of hydrogen-bond-donating (i.e., CH_3OH) and those that cannot (i.e., CH_3CN, and CH_2Cl_2). As CH_3OH has been shown to bind well to the Zr_6-oxo-hydroxo nodes of UiO-66 through an extensive network of hydrogen bonds,[32, 44] we hypothesize that it may provide an additional "knob" for tuning the reactivity of these nodes.

Activity of the catalysts and computational study

As expected, our three UiO-66 derivatives and the isolated Zr_6-oxo-hydroxo cluster[2, 60] (capped with benzoate ligands, as a positive control[10]) were all catalytically active for the oxidation of sulfide in CH_3OH (Fig. 1a). The negative control experiments (i.e., without catalyst or in the presence of bulk ZrO_2) did not show any significant product formation, consistent with previous reports (Fig. 1a).[24] Notably, **decap-UiO-66**, the material with the highest number of open sites on the nodes, has better activity than the other two UiO-66 materials (Fig. 1a, cf the reaction profiles for **decap-UiO-66** vs. **BzOH-UiO-66** and **HCOOH-UiO-66**). As Zr-μ_1-OH moieties in a Zr^{IV}-containing zeolite[61] have been reported to form a combination of Zr-μ_1-OOH and Zr(η^2-O_2) active species in the presence of H_2O_2, it is reasonable to expect that the Zr-μ_1-OH groups on the open sites of our UiO-66 derivatives could similarly be converted to these groups. The resulting catalytically active species would then promote the oxidation of methyl phenyl sulfide to the corresponding sulfoxide (1st oxidation) and eventually to the sulfone (2nd oxidation), which is observed as a second product in the sulfide oxidation (Fig. 1b).

Our DFT calculations, carried out with a single Zr_6-oxo-hydroxo cluster possessing *one* open site [μ_1-OH + μ_1-OH_2, support the idea that the Zr-μ_1-OH pre-catalyst moieties on the Zr_6-oxo-hydroxo nodes are preferentially transformed into active Zr-μ_1-OOH intermediates in the presence of H_2O_2.[62] As shown in Fig 2, the free energy barrier for this activation is 74 kJ/mol (blue profile), consistent with a reaction that can take place at room temperature. The DFT calculations additionally confirm that these Zr-μ_1-OOH active species can catalyze the oxidation of sulfide to sulfoxide and the subsequent overoxidation to sulfone. The free-energy profile of the catalyzed reaction in Fig. 2 (blue profile) shows that the Zr_6-oxo-hydroxo node catalyst reduces the barriers for both stages of oxidation compared to the uncatalyzed reaction (black profile).

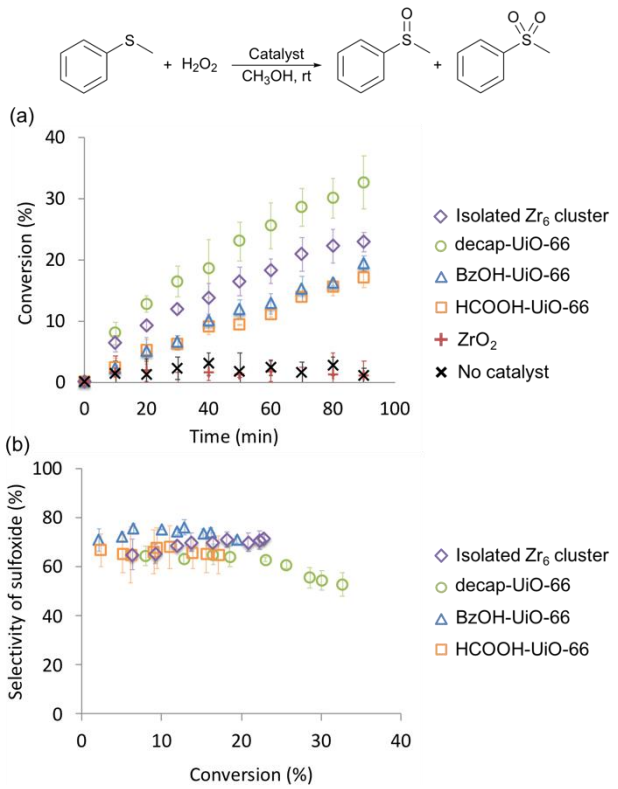

Fig. 1. The conversion (a) and selectivity (b) profiles in the catalytic oxidation of methyl phenyl sulfide in CH_3OH using H_2O_2 as the oxidant. All reactions were carried out with a 100:100:1 molar ratio of sulfide:H_2O_2:Zr_6-oxo-hydroxo clusters. See ESI,† Fig. S12-S14 for catalysis data that extend up to 9 h.

Similar to the sulfide-oxidation activity trend, **decap-UiO-66** also has the best activity for sulfoxide oxidation among the three MOF catalysts, as shown in Fig. 3. However, while the observed rates for **decap-UiO-66** in both sulfide and sulfoxide oxidations are noticeably larger than those for **BzOH-UiO-66** (Table 2), they are not proportional to the number of open sites that we have engineered into these materials (Table 1). Thus, it appears that the MOF steric environment places restrictions on the magnitude of the differences in rates among these materials. This is not surprising, as UiO-66 has relatively small pore apertures (~6 Å for the "ideal"[63] structure)[12] that restrict access for the large sulfide substrate to the open sites around the Zr_6-oxo-hydroxo node. The observed rates are, therefore, influenced by both the number of open sites and differences in steric crowding at the node among **BzOH-UiO-66**, **HCOOH-UiO-66**, and **decap-UiO-66**.

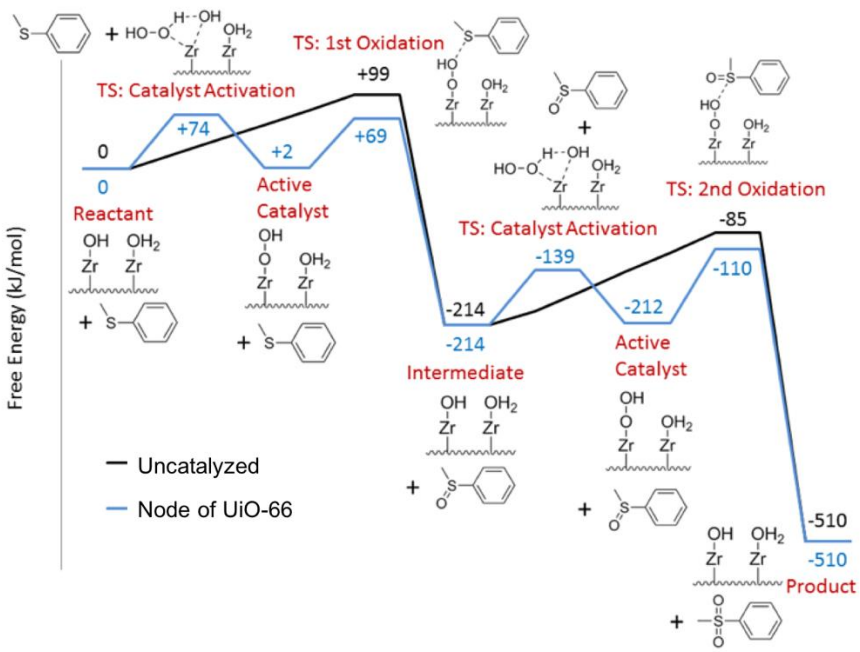

Fig. 2 The computed free energy profiles for the catalytic oxidation of methyl phenyl sulfide using H_2O_2 as the oxidant without catalyst (black) and with a Zr_6-oxo-hydroxo cluster possessing *one* [μ_1-OH + μ_1-OH_2] open site as a model for an "uncapped" node of UiO-66 (blue). To reduce system size in our node model, the capping acid modulator is HCOOH and all benzene rings in the BDC linker are replaced with hydrogen atoms. The system is essentially a ($Zr_6(\mu_3\text{-}O)_4(\mu_3\text{-}OH)_4(OOCH)_{11}$) node. Free energies were calculated at 300 K and are reported in kJ/mol. Results were calculated using the PCM solvation model for CH_3OH for both the uncatalyzed and the catalyzed reactions. In the current figure, only a few selected hydrogen bonds are shown for the transition states to reduce the complexity in the drawings. The reader should note that the simplified depictions of isolated μ_1-OH and μ_1-OH_2 sites are only used in this scheme for clarity. Hydrogen bonds do exist between adjacent μ_1-OH and μ_1-OH_2 sites, as well as with H-bond-capable solvent molecules; thus, isolated μ_1-species are probably unlikely, as discussed in later sections. For detailed illustrations of the hydrogen-bonded species, see ESI,† Fig. S24 as well as the structures shown in Section S9.

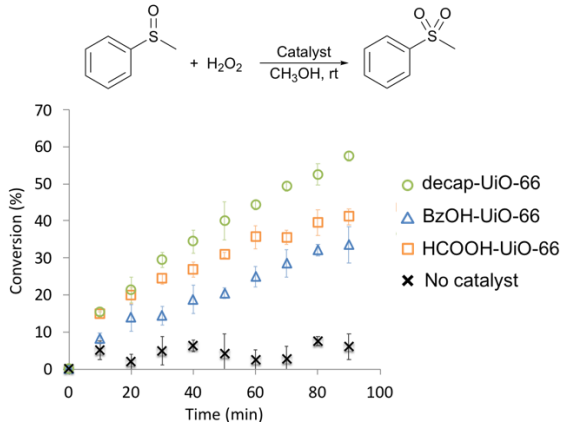

Fig. 3 The conversion profile in the catalytic oxidation of methyl phenyl sulfoxide in CH_3OH using H_2O_2 as the oxidant. All reactions were carried out with a 100:100:1 molar ratio of methyl phenyl sulfoxide:H_2O_2:Zr_6-oxo-hydroxo node.

The free energy profiles in Fig. 2 also predict that the 2nd oxidation in the Zr_6-oxo-hydroxo-catalyzed reaction in CH_3OH has a higher barrier than the 1st oxidation (102 vs 67 kJ/mol, respectively), indicating a slower sulfoxide oxidation step and thus a high sulfoxide/sulfone ratio. This appears to be consistent with the experimental data in CH_3OH solvent, where high sulfoxide selectivities were observed (Fig. 1b). However, when the initial rates for the direct oxidation of sulfoxide (i.e., starting with methyl phenyl sulfoxide as the reactant) were measured, the results (Table 2) suggest that the oxidation of sulfoxide is actually faster than the oxidation of sulfide. It is thus possible that the sulfoxide product may have additional interactions with the open sites, which would increase its oxidation rate beyond the relative 2nd oxidation rate given by the free-energy profile shown in Fig. 2. Supporting this hypothesis is the overall faster oxidation of sulfide catalyzed by **BzOH-UiO-66**[64] in CH_3CN and CH_2Cl_2 (Fig. 4a), along with lower sulfoxide selectivities (Fig. 4b), in comparison to those in CH_3OH. As shown in Fig. 4b, sulfoxide selectivities quickly dropped to 10-15% at 20% conversion, and diminished to almost zero at 30% conversion, suggesting that sulfoxide oxidation in the UiO-66 system is not solely governed by the free-energy landscape shown in Fig. 2.

Table 2 Initial rates for the MOF-catalyzed oxidations of sulfide and sulfoxide in CH_3OH, starting directly with each individual substrate.

Catalyst	Initial rate ($\times 10^{-7}$ M/s)	
	Sulfide oxidation[a]	Sulfoxide oxidation[b]
BzOH-UiO-66	8.3 ± 0.3	16.8 ± 1.3
HCOOH-UiO-66	7.5 ± 1.0	26.4 ± 1.2
decap-UiO-66	14.7 ± 3.1	35.3 ± 3.5

[a]Calculated by linearly fitting the conversion profile of methyl phenyl sulfide below the 20% level. [b]Calculated by linearly fitting the conversion profile of methyl phenyl sulfoxide below the 20% level.

The low sulfoxide selectivity in CH_3CN and CH_2Cl_2 can be explained by a scenario where the sulfoxide product can associate with the active site and be oxidized more readily

than the sulfide, which does not bind to the node. Such a mechanism can be realized in our system if the sulfoxide replaces the OH_2 ligand at the Zr-μ_1-OH_2 site[32, 65] of the Zr_6-oxo-hydroxo nodes.[32, 44] The resulting Zr-μ_1-O=S(CH_3)Ph "intermediate" would serve to increase the local concentration of the sulfoxide next to the active Zr-μ_1-OOH catalytic species and lead to faster sulfoxide oxidation (Scheme 3). In CH_3OH, the labile OH_2 ligand at the Zr-μ_1-OH_2 site would be replaced by CH_3OH and the Zr-μ_1-O=S(CH_3)Ph intermediate is less likely to form. In other words, the local concentration of sulfoxide near the active Zr-μ_1-OOH site in CH_3OH will be lower than those in CH_3CN and CH_2Cl_2 and the free-energy profile in CH_3OH solvent is expected to be quite similar to that shown in Fig. 2 with the Zr-μ_1-OH_2 moiety being replaced by Zr-μ_1-O(CH_3)H species. In such a scenario, the reaction flux would be favored toward the direct reaction of Zr-μ_1-OOH with the sulfide, which has a lower reaction barrier, resulting in higher sulfoxide selectivities.

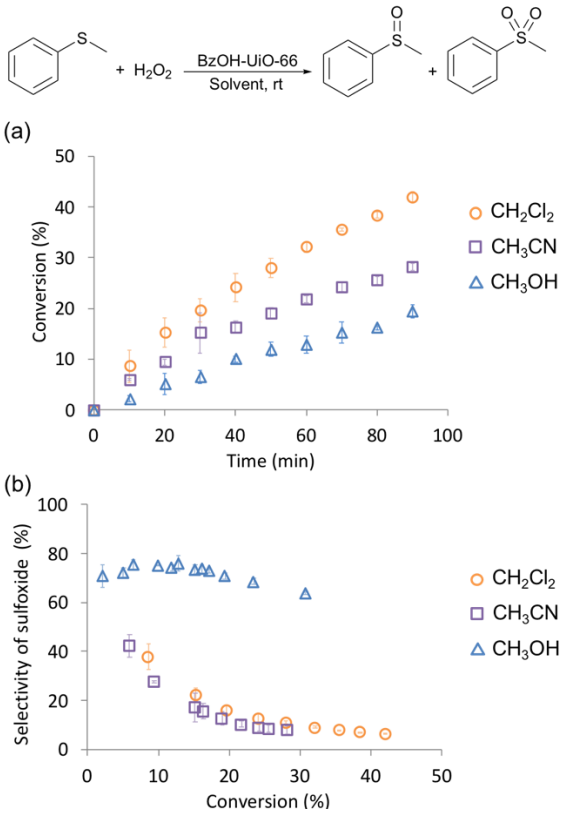

Fig. 4 The conversion (a) and selectivity (b) profiles in the catalytic oxidation of methyl phenyl sulfide using H_2O_2 as the oxidant and BzOH-UiO-66 as the catalyst in three different solvents. All reactions were carried out with a 100:100:1 molar ratio of methyl phenyl sulfide:H_2O_2:Zr_6-oxo-hydroxo node.

Indeed, DFT calculations showed that the O atom of the methyl phenyl sulfoxide product can readily bind to the Zr site adjacent to the Zr-μ_1-OH pre-catalyst species to form a stable [Zr-μ_1-OH + Zr-μ_1-O=S(CH_3)Ph] product intermediate (Fig. 5) that is only about 4.6 kJ/mol higher in energy than the [Zr-μ_1-OH + Zr-μ_1-OH_2] starting species shown in Fig. 2 (Table 3, cf entries 3 and 2). In contrast, the analogous complex between methyl phenyl sulfide and the node could not be found computationally despite an exhaustive search, presumably due to the weaker Zr-S interaction (in comparison to Zr-O binding). For comparison, the CH_3OH-solvated [Zr-μ_1-OH + Zr-μ_1-O(CH_3)H] species, which should predominate in CH_3OH, is very similar in binding energy to the [Zr-μ_1-OH + Zr-μ_1-OH_2] open site precatalyst, suggesting that it can compete effectively against the formation of the aforementioned [Zr-μ_1-OH + Zr-μ_1-O=S(CH_3)Ph] product intermediate (Table 3, cf entries 3 vs. 1 and 2) and prevent overoxidation. As both CH_3CN and CH_2Cl_2 have much weaker interactions with the node than methyl phenyl sulfoxide (Table 3, cf entries 5 and 6 vs. 3), the [Zr-μ_1-OH + Zr-μ_1-O=S(CH_3)Ph] product intermediate would dominate, leading to lower sulfoxide selectivity. We note with interest that because sulfoxide has a similar ΔG_{bind} value to that of CH_3OH (Table 3, cf entries 1 and 3), it can compete effectively for binding to the node, leading to a higher observed rate for sulfoxide oxidation in CH_3OH solvent than sulfide (Table 2), which does not bind.

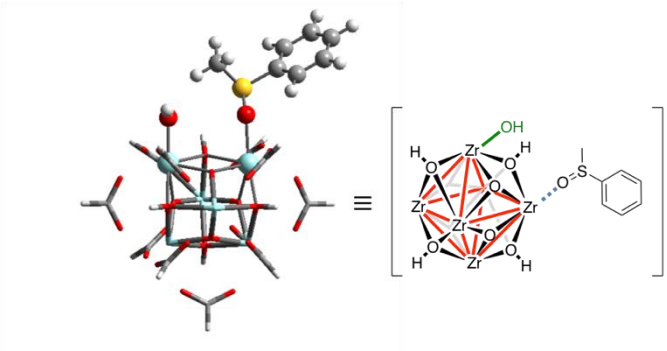

Fig. 5 Optimized structure of the [Zr-μ_1-OH + Zr-μ_1-O=S(CH_3)Ph] product intermediate. White, grey, red, yellow, and cyan spheres represent H, C, O, S, and Zr atoms, respectively.

Table 3 Computed binding free energies at 298 K and equilibrium binding constants of different solvents and reactants to the Zr_6-oxo-hydroxo node.

Entry	Solvent/Substrate	ΔG_{bind} (kJ/mol)	K_{bind}
1	CH_3OH	-34.5	1.1×10^{6}
2	H_2O	-31.2	3.0×10^{5}
3	Methyl phenyl sulfoxide	-26.6	4.6×10^{4}
4	Methyl phenyl sulfone	-8.8	3.5×10^{1}
5	CH_3CN	+8.5	3.2×10^{-2}
6	CH_2Cl_2	+21.3	1.9×10^{-4}

Inhibition by CH_3OH and the possibility of forming H-bonding networks at the Zr_6-oxo-hydroxo nodes

As mentioned earlier, the rate of sulfide oxidation in CH_3OH is slower than in CH_3CN and CH_2Cl_2 (Fig. 4a), and this indicates an inhibitory effect by CH_3OH. Complementary to the free-energy landscape shown in Fig. 2, such an effect can be partially attributed to the ability of CH_3OH to interact with the Zr-μ_1-OH moiety via hydrogen bonding, thus competing with H_2O_2 for interactions with the node and preventing the formation of the Zr-μ_1-OOH active catalyst (Scheme 3). In addition, the slower rate in CH_3OH may also be a consequence of a more extensive hydrogen-bonding network, where 2-4

CH_3OH molecules interact with both sites in the [Zr-μ_1-OH + Zr-μ_1-OH_2] combination (Scheme 3), as proposed by Caratelli et al[32, 65] and recently reviewed by Schubert.[66] Both of these pathways would not exist in CH_3CN and CH_2Cl_2 as these aprotic solvents do not have H-bond-donating capability.

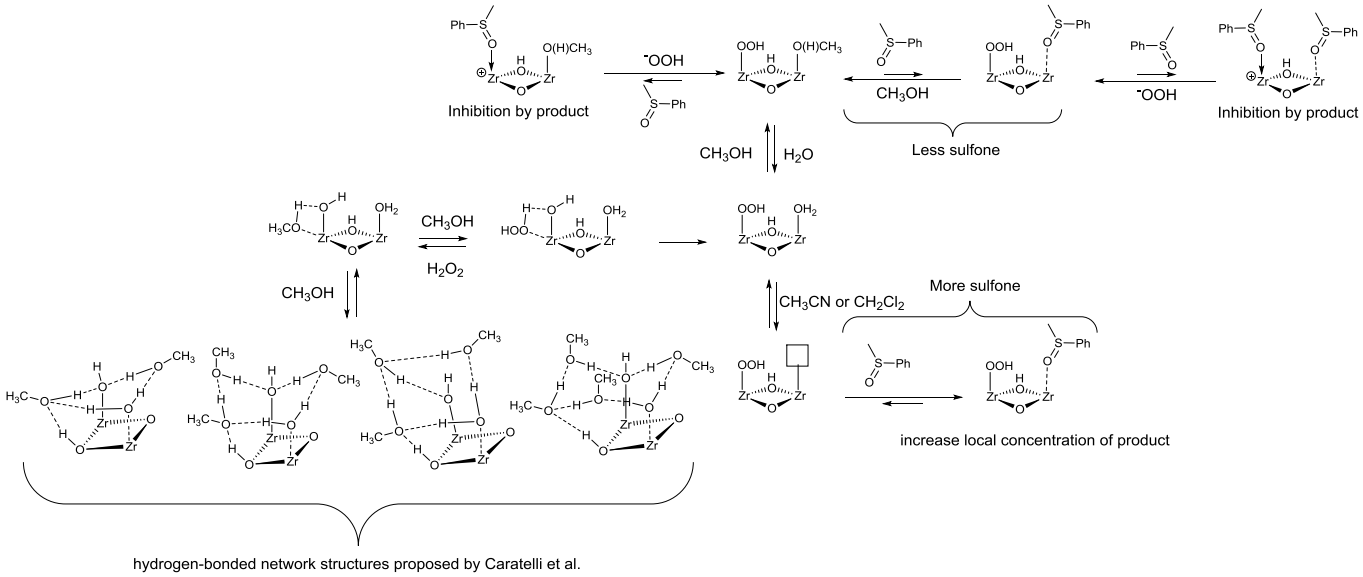

Scheme 3. Proposed interactions of the open sites on the nodes of UiO-66 MOFs with different solvents and substrates. In CH_3CN and CH_2Cl_2 (bottom right quadrant), the [Zr-μ_1-OH + Zr-μ_1-O=S(CH_3)Ph] product intermediate can form and produce more sulfone. In CH_3OH, the reaction can be slowed down due to formation of several CH_3OH-solvated species (left side; the species shown in the bottom left were proposed by Caratelli et al.[32, 65]) that "siphon off" the Zr-μ_1-OOH active species. In addition, [Zr-μ_1-OH + Zr-μ_1-O(CH_3)H] species would predominate in the reaction mixture, reducing the formation of sulfone. Finally, as more product is made, product inhibition may occur (top left and top right) in polar solvents and under low-oxidant conditions such as chosen for this study.

Together, our experimental and computational data support the hypothesis that sulfoxide coordination to the Zr site adjacent to the Zr-μ_1-OOH species can play an important role in CH_3CN and CH_2Cl_2, resulting in more overoxidation and lower sulfoxide selectivity. They also partly explain why sulfone was always obtained as the major product when the UiO-66-catalyzed oxidations of thiophene and its derivatives were conducted in CH_3CN and under high-oxidant conditions.[24-27] In addition to the sulfoxides of thiophenic substrates being more easily converted to sulfone than our methyl phenyl sulfide substrate,[59] the higher probability for the formation of sulfoxide-node complexes in CH_3CN would also promote overoxidation, especially in the presence of excess oxidant.

We note in passing that the high stability of the [Zr-μ_1-OH + Zr-μ_1-O=S(CH_3)Ph] product intermediate (Table 3, entry 3) may make it tempting to imagine a Langmuir-Hinshelwood-type mechanism where the bound sulfoxide (Fig. 5) can interact with the adjacent active Zr-μ_1-OOH site for conversion to the sulfone. However, our DFT calculations show that the formation of a direct Zr-μ_1-OOH•S(O)PhMe complex has a much higher barrier (166 kJ/mol, ESI,† Fig. S23). Incorporation of H_2O_2 into the precatalyst can lower this barrier (to 147 kJ/mol, ESI,† Fig. S23) through the formation of a hydrogen-bonded Zr-OH•(H_2O_2)•S(O)PhMe•Zr intermediate. However, this is still quite high when compared to the direct barrier for sulfoxide oxidation (Fig. 2), preventing it from playing a significant role. As such, we suspect that a Langmuir-Hinshelwood-type mechanism is unlikely.

Recyclability of BzOH-UiO-66 and decap-UiO-66

Both **BzOH-UiO-66** and **decap-UiO-66** can be recovered and re-used for several cycles under our chosen reaction conditions. Not surprisingly, their selectivity profiles (ESI,† Fig. S17 and S19), do not vary significantly over five cycles. Slight decreases in the initial rates of product formation were observed after the 4th cycle (ESI,† Fig. S16 and S18), due to either small amounts of catalyst losses during the recovery process and/or a slight catalyst degradation. The latter is supported by PXRD data (ESI,† Fig. S20 and S21), which indicate that the crystallinities of the catalyst slightly degraded after the first 4 cycles.

The selectivity profiles for both catalysts under repeated recycling closely matched those shown in Fig. 1 and agreed with our proposed mechanistic scheme. Specifically, the selectivity for the **decap-UiO-66** catalyst slightly drops over the allotted reaction time and that for the **BzOH-UiO-66** catalyst remains relatively constant. The former catalyst, having more open sites, is more active and can achieve faster conversion of the sulfide to produce sulfoxide, which in turn would lead to an observable decrease in sulfoxide selectivity. This can easily be understood when one considers that the rate of sulfoxide oxidation is ~2× faster than that for sulfide oxidation (Table 2): as more sulfoxide is produced, the sulfoxide/sulfide ratio increases and the sulfoxide oxidation will become more dominant, leading to a reduction in the sulfoxide selectivity.

Conclusions

In summary, we reported the post-synthesis modifications of **BzOH-UiO-66** to increase the number of open precatalyst sites (i.e., those that are terminated with [Zr-μ_1-OH + Zr-μ_1-OH_2]), achieving a maximum number of up to 5 per node. We observed higher catalytic activities in both sulfide and sulfoxide oxidation with the catalysts possessing higher numbers of open sites. Computational modeling reveals that the labile Zr-μ_1-OH groups on the open sites are likely to be converted into Zr-μ_1-OOH species that are active in oxidizing the sulfide as well as its sulfoxide product. Notably, reactions carried out in CH_3OH solvent can lead to higher selectivities for the sulfoxide product while overoxidation to sulfone predominates in CH_3CN and CH_2Cl_2 solvents. Kinetic studies and computational evaluations support a model where the sulfoxide product can bind to a site adjacent to the active catalyst species in these latter solvents, resulting in higher degrees of overoxidation through increased local concentration. Such an effect is minimized in CH_3OH solvent, which can interact more strongly with the open sites on the nodes than sulfoxide does and thus maintain good sulfoxide selectivity.

Together, our combined experimental and computational study shows that monocarboxylate-capped missing-linker defects on the Zr_6-oxo-hydroxo node of UiO-66 MOFs can be converted into unsaturated coordination sites that serve as good catalysts. Given the recent surge of interests in the "defect engineering" of MOFs,[23, 37, 43, 45, 50, 67-71] these insights may enable researchers to design MOF materials with well-defined defects that can be utilized for a broad range of applications.

Conflicts of interest

R.Q.S. has a financial interest in the start-up company NuMat Technologies, which is seeking to commercialize metal-organic frameworks.

Acknowledgements

This work was supported by the US Department of Energy, Office of Basic Energy Sciences, Chemical Sciences, Geosciences, and Biosciences Division through a grant (DE FG02-03-ER15457) to the Institute of Catalysis for Energy Processes (ICEP) at Northwestern University (assistantship for R.L.). R.L. additionally acknowledges Sigma Xi for a Grants-in-Aid of Research (G201603152055000) award and support from Northwestern University as a teaching fellow. S.T.N. and H.C. acknowledge support from DTRA (HDTRA1-14-1-0014). R.Q.S. acknowledges support from DTRA (HDTRA1-18-1-0003). M.L.M. acknowledges support from a Ryan Fellowship from the Northwestern University International Institute for Nanotechnology and the National Defense Science and Engineering Graduate (NDSEG) Fellowship Program (32 CFR 168a). M.L. acknowledges summer and academic-year research grants from Northwestern University (NU).

NMR and PXRD experiments were carried out at the Integrated Molecular Structure Education and Research Center (IMSERC); SEM images were obtained at the EPIC facility of the Northwestern University Atomic- and Nanoscale Characterization Experimental center. These facilities have received support from one or more of the following sources: the Soft and Hybrid Nanotechnology Experimental (SHyNE) Resource (NSF ECCS-1542205); the MRSEC program (NSF DMR-1720139) at the Materials Research Center; the International Institute for Nanotechnology (IIN); the Keck Foundation; and the State of Illinois, through the IIN. ICP-OES analyses were carried out at the Quantitative Bio-element imaging center (QBIC) at NU. We thank Prof. Mercouri Kanatzidis for the use of the adsorption instrument. This research used resources of the National Energy Research Scientific Computing Center (NERSC), a DOE Office of Science User Facility supported by the Office of Science of the U.S. Department of Energy (DE AC02-05CH11231), and the Quest high-performance computing facility at Northwestern University.

References

1. C. Artner, M. Czakler and U. Schubert, *Inorg. Chim. Acta*, 2015, **432**, 208-212.
2. G. Kickelbick, P. Wiede and U. Schubert, *Inorg. Chim. Acta*, 1999, **284**, 1-7.
3. P. Piszczek, A. Radtke, A. Grodzicki, A. Wojtczak and J. Chojnacki, *Polyhedron*, 2007, **26**, 679-685.
4. G. Kickelbick and U. Schubert, *Chem. Ber.*, 1997, **130**, 473-478.
5. F. R. Kogler, M. Jupa, M. Puchberger and U. Schubert, *J. Mater. Chem.*, 2004, **14**, 3133-3138.
6. U. Schubert, *Chem. Mater.*, 2001, **13**, 3487-3494.
7. U. Schubert, *Chem. Soc. Rev.*, 2011, **40**, 575-582.
8. I. L. Malaestean, M. Speldrich, A. Ellern, S. G. Baca and P. Kogerler, *Dalton Trans.*, 2011, **40**, 331-333.
9. I. L. Malaestean, M. Kutluca, M. Speldrich, A. Ellern and P. Kögerler, *Inorg. Chim. Acta*, 2012, **380**, 72-77.
10. F. Faccioli, M. Bauer, D. Pedron, A. Sorarù, M. Carraro and S. Gross, *Eur. J. Inorg. Chem.*, 2015, **2015**, 210-225.
11. Y. Bai, Y. Dou, L.-H. Xie, W. Rutledge, J.-R. Li and H.-C. Zhou, *Chem. Soc. Rev.*, 2016, **45**, 2327-2367.
12. J. H. Cavka, S. Jakobsen, U. Olsbye, N. Guillou, C. Lamberti, S. Bordiga and K. P. Lillerud, *J. Am. Chem. Soc.*, 2008, **130**, 13850-13851.
13. S. J. Garibay and S. M. Cohen, *Chem. Commun.*, 2010, **46**, 7700-7702.
14. L. Li, S. Tang, C. Wang, X. Lv, M. Jiang, H. Wu and X. Zhao, *Chem. Commun.*, 2014, **50**, 2304-2307.
15. H.-L. Jiang, D. Feng, T.-F. Liu, J.-R. Li and H.-C. Zhou, *J. Am. Chem. Soc.*, 2012, **134**, 14690-14693.
16. D. Feng, Z.-Y. Gu, Y.-P. Chen, J. Park, Z. Wei, Y. Sun, M. Bosch, S. Yuan and H.-C. Zhou, *J. Am. Chem. Soc.*, 2014, **136**, 17714-17717.
17. D. Feng, K. Wang, J. Su, T. F. Liu, J. Park, Z. Wei, M. Bosch, A. Yakovenko, X. Zou and H. C. Zhou, *Angew. Chem., Int. Ed.*, 2015, **54**, 149-154.
18. O. V. Gutov, W. Bury, D. A. Gomez-Gualdron, V. Krungleviciute, D. Fairen-Jimenez, J. E. Mondloch, A. A.

Sarjeant, S. S. Al-Juaid, R. Q. Snurr, J. T. Hupp, T. Yildirim and O. K. Farha, *Chem. Eur. J*, 2014, **20**, 12389-12393.
19. T. C. Wang, W. Bury, D. A. Gómez-Gualdrón, N. A. Vermeulen, J. E. Mondloch, P. Deria, K. Zhang, P. Z. Moghadam, A. A. Sarjeant, R. Q. Snurr, J. F. Stoddart, J. T. Hupp and O. K. Farha, *J. Am. Chem. Soc.*, 2015, **137**, 3585-3591.
20. H. Furukawa, F. Gándara, Y.-B. Zhang, J. Jiang, W. L. Queen, M. R. Hudson and O. M. Yaghi, *J. Am. Chem. Soc.*, 2014, **136**, 4369-4381.
21. W. Morris, B. Volosskiy, S. Demir, F. Gándara, P. L. McGrier, H. Furukawa, D. Cascio, J. F. Stoddart and O. M. Yaghi, *Inorg. Chem.*, 2012, **51**, 6443-6445.
22. K. M. Choi, H. M. Jeong, J. H. Park, Y.-B. Zhang, J. K. Kang and O. M. Yaghi, *ACS Nano*, 2014, **8**, 7451-7457.
23. C. Ardila-Suarez, S. Perez-Beltran, G. E. Ramirez-Caballero and P. B. Balbuena, *Catal. Sci. Technol.*, 2018, **8**, 847-857.
24. C. M. Granadeiro, S. O. Ribeiro, M. Karmaoui, R. Valenca, J. C. Ribeiro, B. de Castro, L. Cunha-Silva and S. S. Balula, *Chem. Commun.*, 2015, **51**, 13818-13821.
25. X. Zhang, P. Huang, A. Liu and M. Zhu, *Fuel*, 2017, **209**, 417-423.
26. G. Ye, H. Qi, X. Li, K. Leng, Y. Sun and W. Xu, *ChemPhysChem*, 2017, **18**, 1903-1908.
27. G. Ye, D. Zhang, X. Li, K. Leng, W. Zhang, J. Ma, Y. Sun, W. Xu and S. Ma, *ACS Appl. Mater. Interfaces*, 2017, **9**, 34937-34943.
28. T. L. H. Doan, T. Q. Dao, H. N. Tran, P. H. Tran and T. N. Le, *Dalton Trans.*, 2016, **45**, 7875-7880.
29. F. Vermoortele, R. Ameloot, A. Vimont, C. Serre and D. De Vos, *Chem. Commun.*, 2011, **47**, 1521-1523.
30. M. J. Katz, R. C. Klet, S.-Y. Moon, J. E. Mondloch, J. T. Hupp and O. K. Farha, *ACS Catal.*, 2015, **5**, 4637-4642.
31. M. C. de Koning, M. van Grol and T. Breijaert, *Inorg. Chem.*, 2017, **56**, 11804-11809.
32. C. Caratelli, J. Hajek, F. G. Cirujano, M. Waroquier, F. X. Llabrés i Xamena and V. Van Speybroeck, *J. Catal.*, 2017, **352**, 401-414.
33. J. F. Blandez, A. Santiago-Portillo, S. Navalón, M. Giménez-Marqués, M. Álvaro, P. Horcajada and H. García, *J. Mol. Catal. A: Chem.*, 2016, **425**, 332-339.
34. Y. Liu, R. C. Klet, J. T. Hupp and O. Farha, *Chem. Commun.*, 2016, **52**, 7806-7809.
35. S. Ling and B. Slater, *Chem. Sci.*, 2016, **7**, 4706-4712.
36. F. Vermoortele, B. Bueken, G. Le Bars, B. Van de Voorde, M. Vandichel, K. Houthoofd, A. Vimont, M. Daturi, M. Waroquier, V. Van Speybroeck, C. Kirschhock and D. E. De Vos, *J. Am. Chem. Soc.*, 2013, **135**, 11465-11468.
37. S. Dissegna, K. Epp, W. R. Heinz, G. Kieslich and R. A. Fischer, *Adv. Mater.*, 2018, **30**, DOI: 10.1002/adma.201704501.
38. In typical oxidative desulfurization model study of diesel fuels, the first stage is "extraction" of a large portion of the sulfur-containing component into a good solvent such as CH_3CN that is also miscible with aqueous H_2O_2. The injection of H_2O_2 to induce oxidation is considered a second stage. The oxidized product is much more soluble in CH_3CN than in the diesel fuel mixture and remains in the former phase. See ref. 24
39. M. E. Davis and R. J. Davis, *Fundamentals of chemical reaction engineering*, McGraw-Hill Higher Education, New York, 2003.
40. S. Cao, F. Tao, Y. Tang, Y. Li and J. Yu, *Chem. Soc. Rev.*, 2016, **45**, 4747-4765.
41. R. Ye, T. J. Hurlburt, K. Sabyrov, S. Alayoglu and G. A. Somorjai, *Proc. Natl. Acad. Sci. U.S.A.*, 2016, **113**, 5159-5166.
42. H. Wu, Y. S. Chua, V. Krungleviciute, M. Tyagi, P. Chen, T. Yildirim and W. Zhou, *J. Am. Chem. Soc.*, 2013, **135**, 10525-10532.
43. M. Taddei, *Coord. Chem. Rev.*, 2017, **343**, 1-24.
44. D. Yang, V. Bernales, T. Islamoglu, O. K. Farha, J. T. Hupp, C. J. Cramer, L. Gagliardi and B. C. Gates, *J. Am. Chem. Soc.*, 2016, **138**, 15189-15196.
45. J. Canivet, M. Vandichel and D. Farrusseng, *Dalton Trans.*, 2016, **45**, 4090-4099.
46. C. A. Trickett, K. J. Gagnon, S. Lee, F. Gándara, H. B. Bürgi and O. M. Yaghi, *Angew. Chem., Int. Ed.*, 2015, **54**, 11162-11167.
47. G. C. Shearer, S. Chavan, J. Ethiraj, J. G. Vitillo, S. Svelle, U. Olsbye, C. Lamberti, S. Bordiga and K. P. Lillerud, *Chem. Mater.*, 2014, **26**, 4068-4071.
48. M. J. Katz, Z. J. Brown, Y. J. Colon, P. W. Siu, K. A. Scheidt, R. Q. Snurr, J. T. Hupp and O. K. Farha, *Chem. Commun.*, 2013, **49**, 9449-9451.
49. A. Schaate, P. Roy, A. Godt, J. Lippke, F. Waltz, M. Wiebcke and P. Behrens, *Chem. Eur. J*, 2011, **17**, 6643-6651.
50. G. C. Shearer, S. Chavan, S. Bordiga, S. Svelle, U. Olsbye and K. P. Lillerud, *Chem. Mater.*, 2016, **28**, 3749-3761.
51. C. Atzori, G. C. Shearer, L. Maschio, B. Civalleri, F. Bonino, C. Lamberti, S. Svelle, K. P. Lillerud and S. Bordiga, *J. Phys. Chem. C.*, 2017, **121**, 9312-9324.
52. O. V. Gutov, M. G. Hevia, E. C. Escudero-Adán and A. Shafir, *Inorg. Chem.*, 2015, **54**, 8396-8400.
53. T. Cottineau, M. Richard-Plouet, J.-Y. Mevellec and L. Brohan, *J. Phys. Chem. C.*, 2011, **115**, 12269-12274.
54. S. Doherty, J. G. Knight, M. A. Carroll, J. R. Ellison, S. J. Hobson, S. Stevens, C. Hardacre and P. Goodrich, *Green Chem.*, 2015, **17**, 1559-1571.
55. H. Srour, J. Jalkh, P. Le Maux, S. Chevance, M. Kobeissi and G. Simonneaux, *J. Mol. Catal. A: Chem.*, 2013, **370**, 75-79.
56. A. Shaabani and A. H. Rezayan, *Catal. Commun.*, 2007, **8**, 1112-1116.
57. A. M. Cojocariu, P. H. Mutin, E. Dumitriu, F. Fajula, A. Vioux and V. Hulea, *Chem. Commun.*, 2008, **44**, 5357-5359.
58. V. Hulea, F. Fajula and J. Bousquet, *J. Catal.*, 2001, **198**, 179-186.
59. M. Bonchio, V. Conte, M. Assunta De Conciliis, F. Di Furia, F. P. Ballistreri, G. A. Tomaselli and R. M. Toscano, *J. Org. Chem.*, 1995, **60**, 4475-4480.
60. N. E. Thornburg, Y. Liu, P. Li, J. T. Hupp, O. K. Farha and J. M. Notestein, *Catal. Sci. Technol.*, 2016, **6**, 6480-6484.
61. D. T. Bregante and D. W. Flaherty, *J. Am. Chem. Soc.*, 2017, **139**, 6888-6898.
62. As Zr_6-oxo-hydroxo clusters have been reported to form oxidation-active $Zr(\eta^2\text{-}O_2)$ intermediates in the presence of H_2O_2 (see reference 10), we also searched for this peroxy intermediate computationally. However, such a species does not appear to be a stable intermediate in our DFT calculations. See ESI,† Section S8 for additional discussion.
63. The "ideal" UiO-66 structure is defined as a structure with the formula $Zr_6O_4(OH)_4(BDC)_6$, that has exactly 6 BDC linker/node (i.e., no missing linker and no capping ligand); see ESI,† Table S1.
64. **BzOH-UiO-66** was selected as the catalyst for this set of studies as it has one open site (Table 1) and can be correlated with the computational work, which employed a model catalyst possessing one [μ_1-OH + μ_1-OH_2] open site.

65. C. Caratelli, J. Hajek, S. M. J. Rogge, S. Vandenbrande, E. J. Meijer, M. Waroquier and V. Van Speybroeck, *ChemPhysChem*, 2018, **19**, 420-429.
66. U. Schubert, *Coord. Chem. Rev.*, 2017, **350**, 61-67.
67. P. Ghosh, Y. J. Colon and R. Q. Snurr, *Chem. Commun.*, 2014, **50**, 11329-11331.
68. D. S. Sholl and R. P. Lively, *J. Phys. Chem. Lett.*, 2015, **6**, 3437-3444.
69. A. K. Cheetham, T. D. Bennett, F.-X. Coudert and A. L. Goodwin, *Dalton Trans.*, 2016, **45**, 4113-4126.
70. Z. Fang, B. Bueken, D. E. De Vos and R. A. Fischer, *Angew. Chem., Int. Ed.*, 2015, **54**, 7234-7254.
71. J. Ren, M. Ledwaba, N. M. Musyoka, H. W. Langmi, M. Mathe, S. Liao and W. Pang, *Coord. Chem. Rev.*, 2017, **349**, 169-197.

Elucidating the mechanism of the UiO-66-catalyzed sulfide oxidation: Selectivity and activity enhancements through modifications of the node coordination environment

Rungmai Limvorapitux,[a] Haoyuan Chen,[b] Matthew L. Mendonca,[b] Mengtan Liu,[a] Randall Q. Snurr,[b,*] and SonBinh T. Nguyen[a,*]

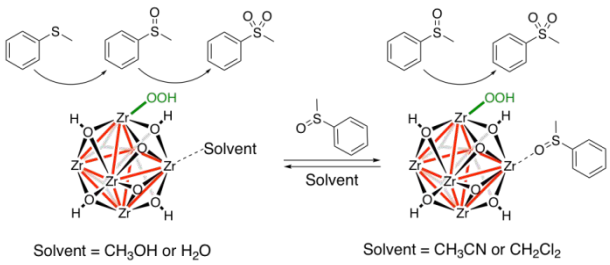

"Open" sites on the UiO-66 Zr_6-oxo-hydroxo cluster node are converted to catalytically active Zr-hydroperoxy species and complexes with solvent/substrate molecule.